Pergamon

VAPOUR CHANNELS IN BOILING, UNCONSTRICTED PARTICLE BEDS—EFFECT ON THE DRYOUT HEAT FLUX

A. K. STUBOS and J.-M. BUCHLIN†

von Karman Institute for Fluid Dynamics, Ch. de Waterloo 72, 1640 Rhode-St-Genese, Belgium

Abstract—The behaviour of vapour channels traversing the upper part of a boiling, unconstricted debris bed is investigated. The presence of such discrete paths facilitates the vapour flow and therefore affects the coolability of the system. On the basis of an extensive experimental support the formation, population density, extent and stability of channels are discussed, leading to the development of a theoretical model for the dryout heat flux in a channelled bed. The latter can be categorized as shallow or deep according to the relative extent of the channelled and packed zones in it.

Key Words: internally heated porous media, two-phase flow, critical heat flux, nuclear safety, modelling and experimental validation

INTRODUCTION

The thermohydraulics of porous media saturated with multiple fluid phases is a topic related to many applications, including the drying of porous solids, geothermal energy production, thermally enhanced oil recovery, the design of heat pipes and capillary pumps, underground high-level nuclear energy disposal and post accident heat removal (PAHR). This last application, addressed to the nuclear safety analysis of liquid-metal fast breeder (LMFBR) and water-cooled reactors, is the main concern of the present paper.

The PAHR scenario describes the sequel to a hypothetical severe accident leading to core meltdown. In such a case, as suggested by experimental evidence, molten core materials will rapidly quench, freeze and fragment upon contact with sodium or water coolant. These fragments may settle on specially designed horizontal surfaces (core catchers) or on the bottom of the reactor vessel, forming unconsolidated matrices of liquid coolant and solid fuel/steel particles known as debris beds. Due to highly radioactive materials within the fuel, the core debris generates heat and the subsequent temperature increase could threaten the integrity of the containment structure if the *in situ* coolability of the debris bed is not adequately assured in the long term (Joly & Le Rigoleur 1979).

At relatively low heat generation rates passive heat removal is achieved by thermal conduction, possibly enhanced by single-phase natural convection. At higher bed power levels the boiling point of the coolant may be reached and the phase change occurring is a very efficient internally cooling process which, unfortunately, is also self-limiting in the case of the PAHR situation: the generation of high vapour flow rate prevents the replenishment of the porous matrix by the inflowing liquid and subsequently dryout occurs. The onset and evolution of a dry zone in the bed mark a sharp change in its coolability because high-temperature gradients are expected due to the rather poor heat removal capabilities of the dried bed portion. Therefore, the prediction of dryout is held to be an important safety issue in the PAHR context, as it may indicate the potential for failure of containment boundaries.

The complex thermohydraulic behaviour of the debris bed is sketched in figure 1. The different characteristic regions and the associated heat transfer modes are identified. For the sake of generality top- and bottom-cooled beds are considered. As the top surface of the bed is maintained at constant temperature by the overlying liquid coolant layer, the first upper zone is subcooled. Heat transfer by conduction and single-phase convection may take place. The top boiling zone

---

†To whom all correspondence should be addressed.

forms as saturation conditions are reached. It is assumed isothermal and characterized by counter-
or co-current two-phase flow. Dryout occurs when the downcoming liquid cannot replenish the
porous matrix due to high vapour production, and the liquid fraction s (also called saturation)
drops locally to zero. The poor effective thermal conductivity of the dry zone leads to rather high
temperature gradients in this region. Bottom booling divides the bed through an adiabatic plane
located inside it and induces the formation of a bottom-subcooled zone separated from the dry
region by a second boiling regime. Due to the small size of the particles (typical effective particle
diameter of 200–400 μm for the LMFBR case of interest here), capillarity overcomes buoyancy
and downward boiling occurs.

To date, in most of the related studies, the above physical model has been applied to debris beds
that have been considered as fixed, randomly distributed arrays of particles. However, both
out-of-pile and in-pile tests have evidenced enhanced bed coolability as a result of natural or
provoked, stable or unstable self-restructuring processes (Stevens & Trenberth 1982; Barleon et al.
1984; Buchlin & Van Koninckxloo 1986). In fact, the situation depicted in figure 1 holds true as
long as the vapour is not able to reach the top of the bed. In the opposite case (saturated liquid
pool or small top-subcooled zone) the vapour escaping the upper part of the boiling particulate
opens discrete, low-resistance paths as shown in the visualization of figure 2. A number of channels
with a diameter 1 order of magnitude larger than the average particle diameter traverse the top
bed region of length L_c (to be called channel length in the following). In this regime the vapour
moves through the channels, whereas the pores are filled with the downcoming liquid. Visualiza-
tions using transparent solid material and dye in the liquid have confirmed this fact (Gabor et al.
1972) and have further shown that channels of the same size occur also in the bed interior, implying
that their formation is not restricted close to the wall only.

The presence of such discrete vapour channels is suggested by the porous flow equations
themselves when the top boundary condition of the bed is examined (Reed 1986). Indeed, the
relatively large bubbles observed leaving the bed indicate that the pressure difference between the
liquid and the vapour (i.e. the capillary pressure) at the bed top is quite small. This, in turn, means
that the liquid fraction is almost equal to unity and implies that the area available for the flow
of the vapour at the top of the bed is practically zero, i.e. the vapour velocity must approach infinity
at this point. Thus, there must be some mechanism like channels to provide for reasonable vapour
exit velocities. Moreover, the existence of channels results in a reduction of the total pressure drop
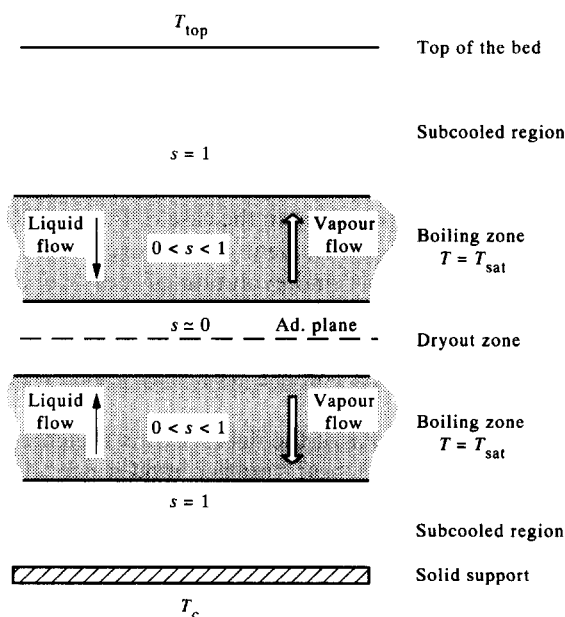required for the vapour flow through the particulate.

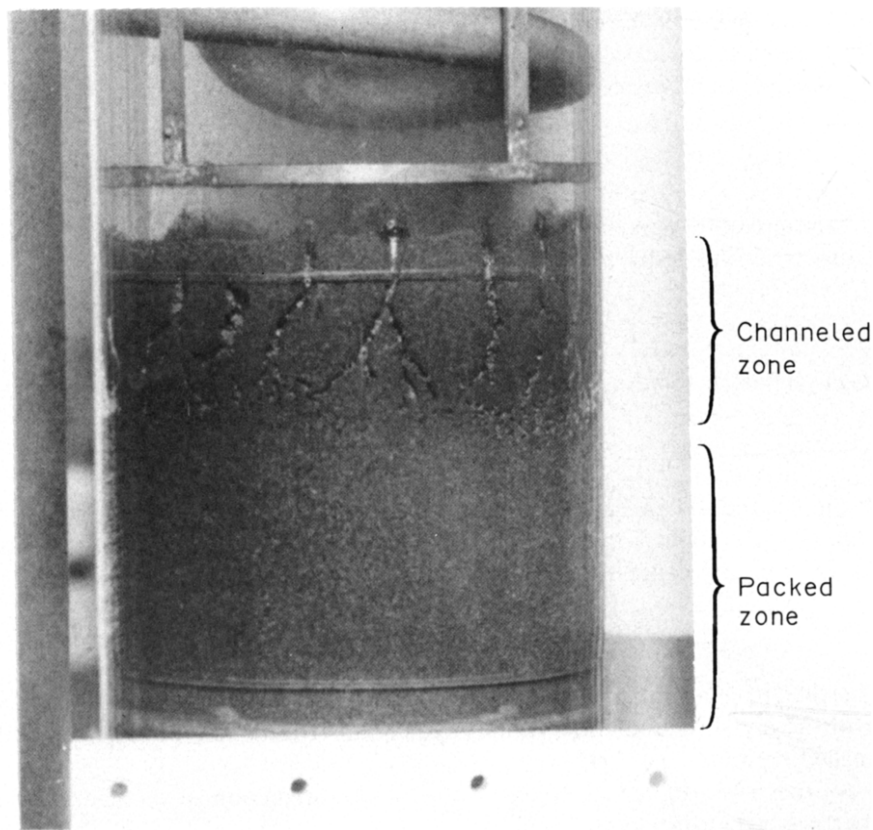Figure 1. Thermohydraulic zones in the debris bed.

Figure 2. Channel visualization in a heat-dissipating debris bed.

The top-subcooled region for water-cooled beds is expected to be thin enough to allow early penetration of vapour, i.e. channels. But this region becomes much thicker in beds saturated with the highly conductive liquid sodium, thus prohibiting the occurrence of channels for power levels up to dryout (Stubos 1990). In this last case the formation of channels has to be provoked, as opposed to the natural channel formation of out-of-pile tests, by disrupting events that lead to disturbances in the packing. A typical example is the deliberate sudden vapour generation, after a power ramp, that is supposed to simulate the initial stages of the debris bed formation in a real accident case, when the particles are still highly radioactive.

During in-pile tests conducted at Sandia Laboratories [D4 (Gronager et al. 1981) and D10 (Mitchell et al. 1984)] and the Mol Nuclear Center in Belgium [PIRAMID-1, Joly et al. (1988)] some states of increased coolability were observed and attributed to vapour channel formation. This indirect evidence of channelling was brought about after disruptive events like superheat flashing or sudden vapour production due to fast power transients. In some cases (the D4 test), the dryout power for an extremely subcooled sodium pool is less than that for sodium with less subcooling, a fact attributed to the collapse of vapour channels (Schwalm & Nijsing 1982; Benocci et al. 1982). However, in the absence of an adequate model for channel behaviour, this and other speculations about the in-pile measurements have not been proven.

Channel Length Models

Following the observations on channelling made in a number of out-of-pile tests, a model to estimate the channel length eluded researchers for over a decade.

A qualitative analogy between spouting of fluidized powder and channelling has been exploited in a semi-empirical way by Buchlin et al. (1983). Naik & Dhir (1982) used a pipe flow formulation for the vapour flow in the channels and obtained experimental data on the shape and number of channels. More recently, Schwalm (1985) and Barleon et al. (1985), as well as Mehr & Wurtz (1985), suggested modelling the channelled region as a porous layer of higher permeability to vapour flow.

In fact, the modelling approach commonly adopted (Jones *et al.* 1982; Schwalm & Nijsing 1982) is exemplified by Lipinski's model (1982). It is assumed that the vapour pressure P_G at the bottom of a channel is sufficient to offset the weight of the overlying particles plus liquid. If P_G is computed from

$$P_c = P_G - P_L = \sigma \sqrt{\frac{\epsilon}{\kappa}} J(s),$$

[1]

with the capillary pressure P_c expressed via the Leverett function J and the liquid pressure considered hydrostatic, this requirement gives

$$L_c = \frac{\sqrt{180}\sigma \cos \theta J}{\epsilon d_p (\rho_s - \rho_L) g},$$

[2]

where the Kozeny relation for the bed permeability κ has been used,

$$\kappa = \frac{d_p^2 \epsilon^3}{180(1 - \epsilon)^2},$$

and ρ, d_p, ϵ, σ and θ stand for the bed density, the mean particle diameter, the porosity, the surface tension and the contact angle, respectively. The Leverett function J is a non-dimensionalized capillary pressure, typically expressed as

$$J = \frac{(s^{-1} - 1)^{0.175}}{\sqrt{5}},$$

and depends on the local saturation value at the channel base. To evaluate this saturation value, the continuity of the pressure gradient is employed as an interfacial condition between the packed and the channelled regions.

A different approach is adopted by Reed (1986) for the prediction of the channel depth. The statics of the particle bed at the channel wall is examined and combined with the capillary pressure curve:

$$L_c = \frac{4.62\sigma \cos \theta}{\epsilon d_p (\rho_s - \rho_L) g}.$$

[3]

As the physical insight offered by the approach is considered to be important for the developments that follow, a more detailed reference to it is made in later sections.

These models present certain shortcomings regarding the formation and extent of channels in out-of-pile (Schwalm 1985) as well as in-pile (Mitchell *et al.* 1984) tests, especially when the expected channel length is large. For example, if the case of the D10 experiment is considered (Mitchell *et al.* 1984), an estimation of the subcooled zone thickness close to unchannelled dryout gives 5.5 cm, while the predicted channel length extends to almost 11 cm, i.e. penetration should have been observed at much lower power levels. In addition, the measured channelled dryout power in the visually inaccessible in-pile tests (Mitchell *et al.* 1984; Joly *et al.* 1988) implies the presence of channels that do not occupy the whole bed, in direct contradiction with the models (Stubos 1990).

These remarks, along with the uncertainties concerning the influence of the vapour channel formation on the coolability of the bed (Barleon *et al.* 1984; Schwalm 1985), stress the fact that, to date, all attempts to quantify the effects of channelling have failed and further refinement of the modelling of channel behaviour is necessary. It is the objective of the present paper to explore the physics of channelling and lead to a reliable model for the dryout heat flux in channelled beds. In a first step, the different possible modes of channel formation are briefly described. Other important issues concerning the density, stability and length of channels are also examined.

A significant contribution to the understanding of the processes involved has resulted from the extensive use of the Opera test facility designed and built at VKI for this purpose (Buchlin & Van Koninckxloo 1986; Stubos 1990). A bed of ferrite particles submerged in water is heated dielectrically up to dryout conditions. The bed height may vary between 10 and 30 cm, while the two classes of particles mainly tested are characterized by effective particle diameters of 320 and 700 μm, respectively. Infrared as well as photographic images of the bed are continuously recorded and used after suitable processing for a quantitative description of the bed behaviour (Buchlin *et al.* 1989). A considerable amount of the data obtained is used in the following sections to validate the proposed modelling for the respective aspects of channelling.
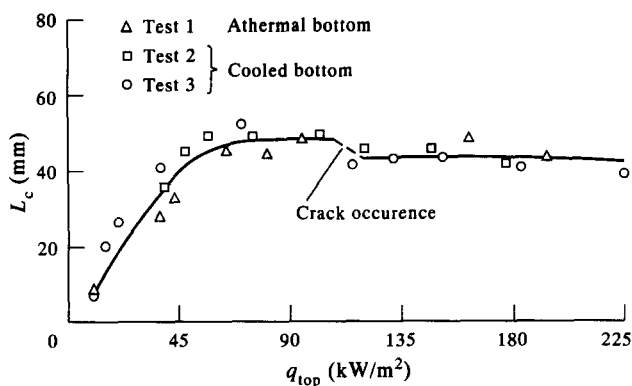
Figure 3. Channel length L_c vs the top heat flux q_{top} in the Opera bed.

CHANNEL FORMATION

Natural Formation

For many years it has been held as a commonly accepted view among researchers (Lipinski 1982; Jones et al. 1982; Schwalm & Nijsing 1982; Reed 1986) that channels penetrate the top-subcooled layer when the expected L_c becomes comparable to its thickness H_{sub}. Expression [2] is widely used to estimate L_c and gives, in many cases, satisfactory predictions for the observed final L_c. However, as already noted, the behaviour of in-pile beds remains unexplained in the sense that penetration is not observed even though the predicted L_c substantially exceeds the measured thickness of the subcooled zone (Mitchell et al. 1984). The example of the D10 in-pile test considered before stresses the existing uncertainty on this point.

The evolution of L_c with the top heat flux is shown in figure 3 for the 320 μm Opera bed. The repeatability of the experimental curve is exemplified by including points from different tests. An incipient L_c value of 7.5–9.0 mm has been observed on several occasions during the experiments. For moderate power levels ($q_{top} < 100$ kW/m^2), the channels extend to 50–55 mm. As the power increases ($q_{top} > 100$ kW/m^2), a slight decrease in L_c to 45 mm is observed accompanied by the appearance of a 10–15 mm thick cracked zone which replaces the bottom part of the channelled region (Buchlin et al. 1989). The final L_c value is found to be independent of the total bed height.

Digital treatment of the infrared images from the same bed permits the study of the evolution of the top-subcooled zone thickness H_{sub} with the top heat flux. This, in conjunction with the recorded video images of the bed, proved to be of great use in revealing, for the first time, the mechanism of channel formation. Indeed as figure 4 shows, soon after incipient boiling, H_{sub} takes its minimum value of 7.2 mm. This marks the onset of channelling in the bed, characterized by an equal incipient L_c. The presence of channels facilitates the cool inflow of liquid and the escape of vapour from the boiling zone. In addition, it means that the power dissipated in the two-phase regime is carried by the vapour all the way to the pool, i.e. it is now removed in parallel with the heat generated in the subcooled layer. Alternatively speaking, the subcooled region has to remove only the power produced in it and this results in its expansion for modest increases of the top heat
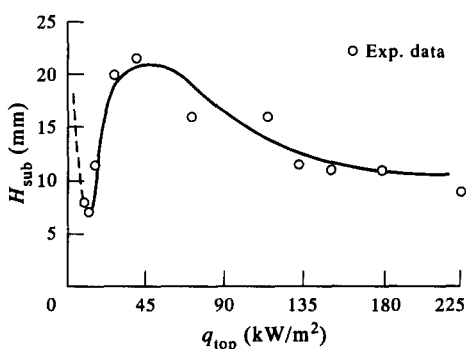
Figure 4. Top-subcooled zone thickness H_{sub} from infrared imaging vs the top heat flux q_{top}.

flux following the channel formation. At higher power levels and after the stabilization of L_c, H_{sub} starts decreasing, as expected, with an asymptotical tendency.

This mechanism for the occurrence and evolution of channels, from a small incipient L_c to the final L_c, offers a plausible explanation for the observed delay in channel penetration during the in-pile tests. Evidently, the thick subcooled zones, due to the presence of liquid sodium (several times thicker than the incipient L_c), suppress channel formation, in contrast to the general belief that channels should occur as soon as H_{sub} becomes comparable with the final extended L_c.

Stubos & Buchlin (1988) included the effect of friction forces on channel formation via a sticking factor S_f, defined as the ratio between the vapour pressure at the channel base and the overlying bed pressure (Lipinski 1984). Semi-empirical expressions for S_f were proposed on the basis of simple experiments to observe the formation and evolution of channels in glass and steel beds. It is concluded that the onset of channelling is governed by rather high S_f values. Therefore, the incipient L_c is predictable and small (of the order of 1–2 cm) and the occurrence of channels, according to the previously described mechanism, can be delayed for higher powers or even suppressed completely (as in the case of in-pile tests). However, once the channels are formed it is much easier for the vapour to lengthen them as its velocity increases with power. This means that S_f decreases rapidly and tends asymptotically to a value close to unity; L_c then reaches its final value given by [2]. The clear distinction between incipient ($S_f > 1$) and evolved channelling ($S_f \approx 1$) allows us to account for the non-occurrence of channels in D10 and other in-pile tests even at high power levels (Stubos & Buchlin 1988).

Provoked Formation

As opposed to this "natural" way of channel formation, several disruptive events may also induce channel penetration in an initially packed bed. Superheat flashing of the liquid, as incipient boiling is approached, or sudden vapour production, after the application of fast power transients, occurred spontaneously or were deliberately provoked at the final stages of recent in-pile experiments. The main reason for this type of investigation is to study the influence of similar phenomena that may occur during the debris bed formation in a real case, because of the expected high rate of heat generation in the initial phase of the accident.

The first out-of-pile simulation of the effects of steep power ramps on the behaviour of the debris bed has been performed using the Opera facility. It was observed that the net result of such events is generally the growth of severe disturbances in the upper bed part that disrupt the packing and cause extended channelling. The mechanism of this "provoked" channel formation is revealed with the help of visualizations (Stubos et al. 1989) and allows for the modelling of channel density, as discussed in a later section. Actually, the large amount of vapour generated suddenly in the boiling region lifts, in a piston like manner, the upper part of the bed, a fact that results in channel penetration caused by Taylor instability. On the basis of this mechanism, and with the help of numerical computations, the in-pile data have been interpreted successfully (Stubos & Buchlin 1993).

One of the most interesting experimental findings in this context is that the bed takes up the same final configuration, in terms of the relative extent of the channelled region, number and distribution of channels etc., independent of the power history. This kind of observation was intuitively expected since the channels are numbered and distributed in an optimal way to reduce the vapour pressure drop requirements, while their final length is determined by factors that are functions of the bed and fluid characteristics only. In other words, channelled dryout is the same regardless of the approach to it (small steps or steep changes in the power input), and the out-of-pile data can be used for the interpretation of in-pile results in this respect.

Data were obtained concerning the number and diameter of channels as well as their distribution on the bed cross-section. After the first appearance of channels their number increases with power until a maximum is reached, in agreement with the observations of Barleon et al. (1984). The channel diameter D_c, however, does not exhibit significant variations and remains around 2.5 mm for all the beds tested. It should be mentioned that all the data reported here are very reproducible, the claim being valid even for the pattern of channels across the bed surface. It is this repeatability and regularity of the observed pattern that gave rise to the idea of modelling it using Taylor instability considerations (Stubos 1990).

CHANNEL DENSITY

The mechanism of channel formation revealed above serves in proposing a physical model for the channel density, which is defined as the number of channels per unit cross-sectional area of the bed. A schematic representation of the top view of the bed with the observed channel pattern is shown in figure 5.

During the power transient the onset of the disturbance is marked by the formation of a vapour-filled crack that separates the bed into two parts. As the vapour slug displaces the overlaying bed upward (unstable configuration), the occurring Taylor instability manifests itself via the wavelike distortion of the interface between the crack and the liquid-filled overlying packing (Stubos & Buchlin 1993). In fact, one may well expect that in this case the Taylor cutoff wavelength, given by linear stability theory, predicts accurately enough the observed channel pattern. The reason is that the initial perturbation at the vapour/bed interface results in the expulsion of particles and the opening of channels, thus freezing the original pattern before non-linearities become dominant.

The channel density N_c in a relatively deep bed, where channels penetrate a significant bed portion but do not extend to the bed bottom, has been found experimentally to depend very weakly on the bed height (Stubos 1990). It can be calculated as (Jones *et al.* 1984):

$$N_{cd} = \frac{1}{\lambda_T^2},$$ [4]

where the spacing between channels λ_T corresponds to the following modified critical Taylor wavelength,

$$\lambda_T = 2\pi \left[\frac{\sigma_e'}{(\rho_e - \rho_G)g} \right]^{0.5}.$$ [5]

Here λ_T is based on an effective bed density $\rho_e = \rho_s(1 - \epsilon) + \rho_L\epsilon$ as well as on an effective interfacial tension coefficient, given by

$$\frac{\sigma_e'}{d_p} = \sigma \cos\theta \sqrt{\frac{\epsilon}{\kappa}} J_{br}$$ [6]

where J_{br} represents the breakthrough value of the Leverett function. Expression [6] implies that the actual interfacial tension is defined by the menisci of liquid in the pores. Moreover, the minimum possible curvature of the perturbed interface between the vapour and the overlying displaced bed should be of the order of the particle diameter, since this is the smallest possible channel diameter, at least at the level of the channel base. It should be noted that presently σ_e' can be approximated as

$$\sigma_e' \approx 8\sigma$$

after substituting the Kozeny formula for κ in [6] and using a porosity value of 0.4 and a J_{br} value of 0.38 (Reed 1986). A similar relation has been proposed by Chuoke *et al.* (1959) who first attempted representing the macroscopic effects of capillarity through such a phenomenological effective coefficient in the case of immiscible displacement processes.
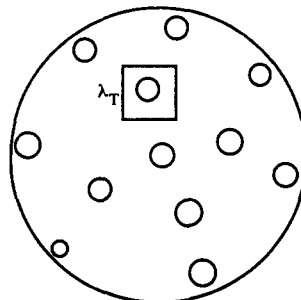

Figure 5. Schematic top view of the bed surface.

Combining [4]–[6] and employing the Kozeny formula for the bed permeability and the breakthrough value of the Leverett function, we obtain:

$$N_{cd} = \frac{0.2(\rho_e - \rho_G)g\epsilon}{4\pi^2\sigma(1-\epsilon)}.$$ [7]

In shallow beds, with channels extending to the bed bottom, it is observed that N_c increases with decreasing bed height (Jones et al. 1984; Stubos 1990). In this case, as well as in the case of channelling confined to the few loose top particle layers of the bed, there exists no sustained contact between the particles in the channelled zone to justify the use of an effective interfacial tension coefficient. Following Dhir & Catton (1977), the channel density in shallow beds can be expressed as

$$N_{cs} = \frac{1}{\lambda_T^2}(1 - CH^*),$$ [8]

where the spacing between channels is now given by

$$\lambda_T = 2\pi \left[\frac{\sigma}{(\rho_e - \rho_G)g}\right]^{0.5}.$$ [9]

Substituting [9] into [8] results in

$$N_{cs} = \frac{(\rho_e - \rho_G)g}{4\pi^2\sigma}(1 - CH^*),$$ [10]

with the bed height H non-dimensionalized by the expected channel length. The estimation of the latter is the subject of the next section.

The shallow-bed relation for the channel density [10] at $H^* = 1$ combined with [7] provides an expression for the "constant" appearing in [10] as a function of the bed porosity:

$$C = 1 - \frac{0.2\epsilon}{1-\epsilon}.$$ [11]

For the typical range of porosities in PAHR debris beds, 0.35–0.5, a value between 0.8 and 0.89 is found and compares favourably with the empirical 0.82 that is computed from the value given by Dhir & Catton (1977). The predictions of the full model for N_c show good agreement with the available shallow-bed data of Jones et al. (1984) as well as with the deep-bed points coming from the present study and the observations of Gabor et al. (1974) and Naik & Dhir (1982), as shown in figure 6. The data originating from channelled zones that extend no farther than the loose top
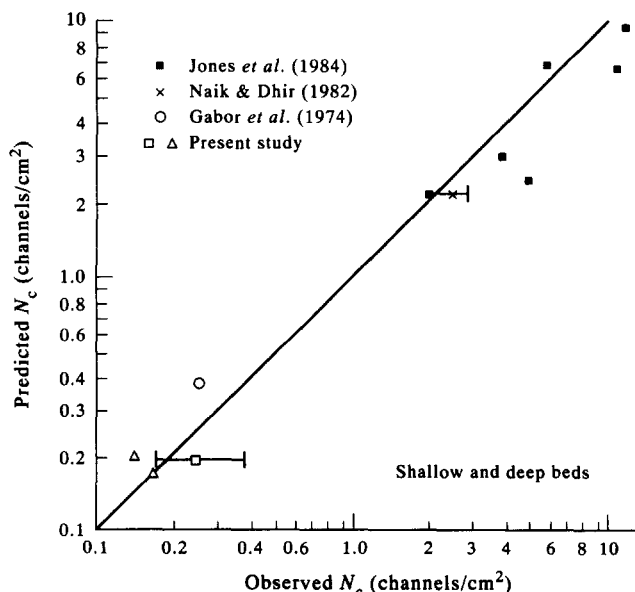

Figure 6. Comparison between predicted and observed channel densities N_c in shallow and deep beds.
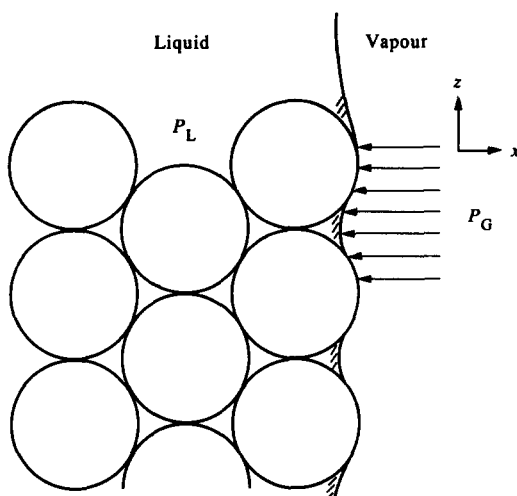
Figure 7. Schematic view of the channel wall (Reed 1986).

layers of debris are approximated by [9], since there is particle motion there and, subsequently, no sustained contact between the particles.

CHANNEL EXTENT AND STABILITY

After examining in detail the conditions under which channels are formed in the debris bed, we proceed to the problem of determining L_c. As will become clear from the following discussion, channel stability must be taken into consideration for a reliable prediction of the extent of the channelled zone.

Channel Extent

It has already been mentioned that the commonly used model for channel depth is Lipinski's (1982) model, expressed by [2] and based on the assumption of vapour pressure offsetting the bed weight at the bottom of the channels. A different approach is adopted by Reed (1986) for the prediction of the extended channel length. A bound is obtained on L_c by examining the geometry of a channel as in figure 7, which is a schematic of a vertical channel wall. The total horizontal normal stress on the solid matrix τ_{xx} is equal to the pressure difference between the vapour and liquid phases, i.e. to the capillary pressure P_c, while the vertical stress produced by the weight of the overlying bed takes the form (Reed 1986):

$$\tau_{zz} = (\rho_s - \rho_L)(1 - \epsilon)gL_c. \tag{12}$$

The shear stress on the channel wall is assumed to be negligible compared to the normal stresses, so that the free-body diagram of an element of the solid matrix can be represented as in figure 8.

For unconsolidated particle beds the failure limits, referring to a collapsing or an expanding channel respectively, are described by the Mohr–Coulomb law as figure 9 shows. Mohr's circles
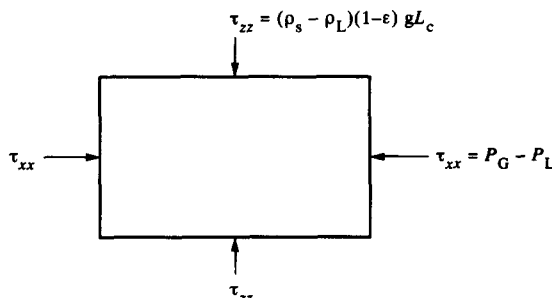

Figure 8. Free-body diagram of an element of the solid matrix (Reed 1986).

that cross the failure curve describe unstable states of stress. A state of impending failure is represented by a Mohr's circle tangent to the curve. For a given value of vertical stress the two possible failure modes, i.e. impending channel collapse and impending channel expansion, are drawn in figure 9 and imply that for a stable configuration (Reed 1986):

$$k_a \tau_{zz} \leqslant \tau_{xx} \leqslant k_p \tau_{zz} \tag{13}$$

or after substitution of [12] and rearrangement that

$$\frac{L_0}{k_p} \leqslant L_c \leqslant \frac{L_0}{k_a}, \tag{14}$$

where

$$L_0 = \frac{P_c}{(\rho_s - \rho_L)(1 - \epsilon)g} \tag{15}$$

and k_a and k_p represent the stress ratio at the two extreme cases of impending channel collapse and expansion, respectively. If it is assumed that the saturation at the bottom of the channelled region can be approximated by the value 0.99, then the capillary pressure is expressed by its breakthrough value on the drainage Leverett curve:

$$P_c(s = 0.99) = 0.38\sigma \cos \theta \sqrt{\frac{\epsilon}{\kappa}}. \tag{16}$$

For a friction angle of 30°, $k_a = 0.33$ and $k_p = 3.0$, [14] yields bounds on L_c that are too far apart. Reed (1986) used experimental information on L_c to infer the state of stress of the solid matrix. A stress ratio of unity fits his data reasonably well, reducing Mohr's circle to a point (figure 9) and implying, in agreement with the initial assumption, that no shear forces exist in any coordinate frame. This means the $L_c = L_0$, i.e. that L_c is given by [3]. Furthermore, the inability of the solid matrix to sustain a shear force statically gives it the appearance of a fluid, although the channelled region is not fluidized in the classical sense (Reed 1986).

Interestingly, there exists a striking similarity between Lipinski's L_c and Reed's prediction [3]. The two relations coincide except for the value of the Leverett function, which Reed assumes as always equal to the breakthrough value. They seem to predict satisfactorily the observed L_c as well as its tendency to increase with increasing surface tension and decreasing particle diameter and solid density (Jones et al. 1982; Reed 1986; Stubos & Buchlin 1988). However, a detailed comparison reveals inadequacies and suggests that consistency between experiment and theory is kept only when the channels involved are not longer than 5–7 cm (Buchlin & Stubos 1987). Indeed, in the case of light particle beds, such as those made by glass beads, most of the tests performed result in long unstable channels, especially when the particles are small in size and the interfacial tension high (e.g. water-saturated beds) (Jones et al. 1982; Campos 1983; Reed 1986). On the other hand, when heavy but very small ($d_p < 200\ \mu$m) particles are used, the observed stable channel depth may be several times lower than the predicted one (Schwalm 1985; Eckert et al. 1985). In addition, the calculated channel length in the case of in-pile tests leads to significant overestimation of the channelled dryout power (Mitchell et al. 1984).
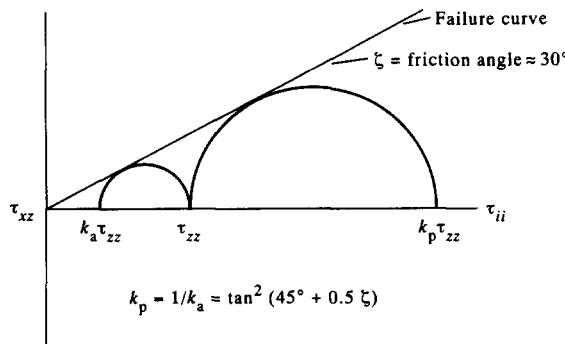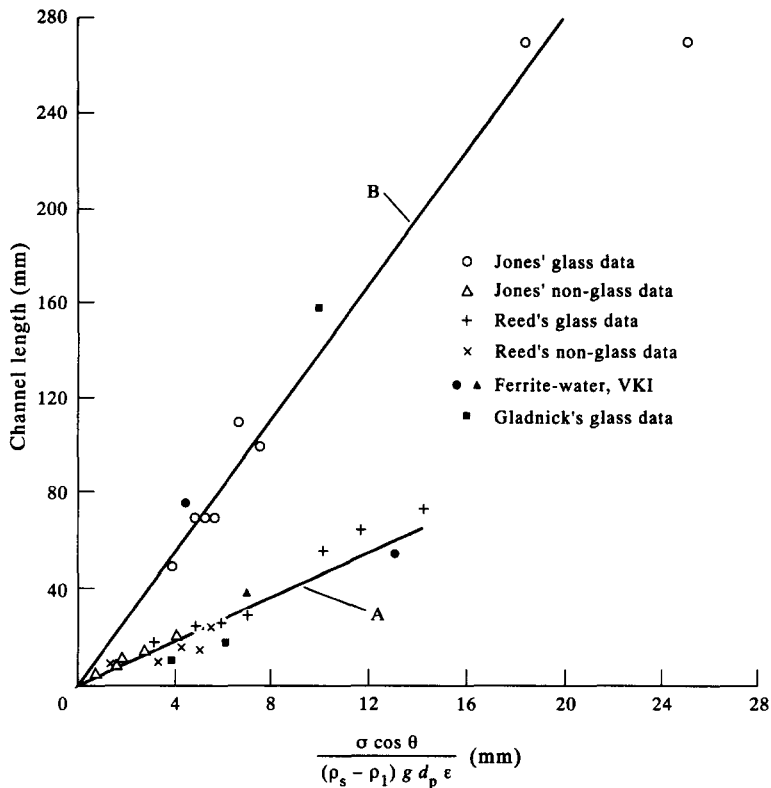

Figure 9. Mohr–Coulomb failure law (Reed 1986).

Figure 10. Measured and predicted channel lengths L_c: (A) [3]; (B) maximum L_c, [14].

From the above discussion the need for further modelling becomes evident. An extension of Reed's (1986) model is attempted first, to include cases where the channel wall shear stress τ_{xz} is not negligible. The mean shear is expressed by the equation:

$$\tau_{xz} = \frac{D_c}{4L_c} \Delta P_G = \frac{\delta C_0 \mu_G V_c}{D_c}, \qquad [17]$$

which refers to laminar flow through a cylindrical tube of diameter D_c with V_c denoting the vapour velocity in the channel. The correlation factor C_0 accounts for the enhancement of the friction coefficient due to the change in the velocity profile caused by vapour injection through the channel wall, the tortuosity of the channel and the possible entrainment of particles by the vapour (Abe et al. 1982). Here the vapour gravity, as well as the momentum change between the inlet and outlet of a channel, have been neglected. The value of C_0 is not known a priori. Naik & Dhir (1982) estimate it as 50, on the basis of experimental information from steel beds with bottom liquid inflow and saturated top. Dhir & Catton (1977) obtain good agreement with the channel density data of Gabor et al. (1974) if they use $C_0 = 20$. For the same range of Reynolds number (laminar), Abe et al. (1982) propose, only as an order of magnitude indication, $C_0 = 10$.

According to [17], as the power increases in a heated bed the vapour velocity may reach values that make τ_{xz} comparable to the vertical stress τ_{zz}, especially in the case of small ρ_s and high porosity (cf. [12]). If, in addition, the bed consists of rather large particles and the liquid is characterized by high surface tension, then the appropriate levels of V_c can be obtained before the onset of dryout in the bed, since under these conditions the dryout power increases considerably. At this point the matrix is no longer in a hydrostatic state of stress and the channel tends to elongate farther. Its maximum attainable length is given by [14].

One might consider the following example. A 0.2 m high bed of ferrite particles ($\rho_s = 4100 \text{ kg/m}^3$) saturated with water is formed in the Opera test section. The bed porosity is 0.48 and the effective particle diameter is 700 μm. At low power levels channels 1.5–4.0 cm in length are observed, the prediction of [3] being 2.65 cm. As this bed fulfils the requirements mentioned above, at a power deposition of about 5.1 kW, well before dryout, the shear stress in a channel amounts to approx.

30% of the vertical stress that would be produced with such small L_c values. At this high power level about 10–12 channels (average $D_c = 2.5$ mm) are observed to traverse the top part of the bed until a depth of 8–9 cm, which has to be compared with the 7.9 cm upper bound suggested by [14].

It seems worth the effort to plot the observations of Reed (1986), Jones et al. (1982) and Gladnick (1985) on beds of glass spheres along with the ferrite–water system used in Opera, and to compare them to Reed's prediction [3] as well as to the upper bound of L_c. As shown in figure 10, and already noted by Reed (1986), the data points appear to be divided into two groups, supporting the present extension of his model. The few points following [3] are those obtained with methanol by Reed (1986) and with water by Gladnick (1985), using quite low gas velocities in both cases. Under these conditions the shear stress never exceeds 2% of the vertical stress and the agreement with [3] is explained.

It should be noted here that the condition of very long channels in the bed brings back into play the $\tau_{xz} \ll \tau_{zz}$ assumption since, thanks to the relatively large L_c, τ_{zz} increases significantly. Therefore, the channelled region again takes the appearance of a fluid but fluidization is now possible because of the large vapour velocity involved.

High vapour velocities in a light particle bed may indeed induce fluidization. This seems to be the case with unexpectedly long channels like those that extend to the bottom of the bed, no matter how deep the latter is—as reported by Campos (1983) in bottom-heated glass beds and Reed (1986) who injected air through glass beads saturated with water. In fact this type of three-phase fluidization is described as inherently unstable by Gabor et al. (1984) and leads to the formation of wide, short-lived channels in the fluidized region that close and re-open sporadically. Convincing evidence about the relevance of fluidization in explaining the behaviour of light debris, when V_G is high enough, comes from Reed's statement that his glass–water combination yielded unstable channels reaching the bottom of the 20 cm deep bed at a gas superficial velocity of more than about 0.2 m/s. For the particle diameters used in these tests, the prediction of the minimum fluidization velocity of the system, according to the empirical correlations of Gabor et al. (1984), ranges between 0.12–0.19 m/s. On the contrary, the same glass beads when used with low surface tension liquids (e.g. methanol) in a thin test section and with almost 1 order of magnitude lower gas velocities did not become fluidized and exhibited stable and predictable channelled zones (figure 10).

Channel Stability

Despite the understanding gained concerning some peculiarities in the behaviour of certain light particle systems, there still exist unresolved questions which dictate the need for further modelling. Heavy particles, like the fuel debris, behave differently from light ones. They follow [3] rather closely as long as the predicted L_c does not exceed a value ranging between 5–7 cm, as several observations suggest (Buchlin & Stubos 1987). In cases where longer channels are expected, i.e. as d_p decreases and/or σ increases, discrepancies are found and the stable channels observed do not extend beyond the aforementioned limit. It should be noted here that, contrary to the case of light
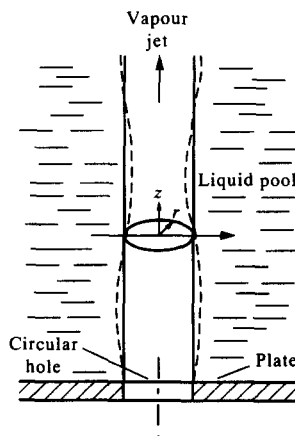

Figure 11. A vapour jet in a liquid pool (Yao & Sun 1982).

particles, the large solid density requires such vapour velocities for fluidization to occur, that the latter is a rare possibility at least for power levels up to dryout. Only with steep power ramps that lead to the sudden generation of large amounts of vapour in the bed may the minimum fluidization velocity be attained (Stubos & Buchlin 1993).

In the case of heavy particles and for the range of V_G reached in PAHR experiments τ_{xz}, given by [17], remains much smaller than τ_{zz} so that Reed's assumption is satisfied and the matrix, though not classically fluidized, exhibits a fluid-like behaviour. This fact permits the investigation of the channel stability according to the idealized physical model of gas jet injected upward from a circular hole of diameter D_c into a large liquid pool, as shown in figure 11. The gas velocity is assumed constant along the jet and this makes the analysis more suitable to the case of channels traversing a subcooled region. A linear stability analysis can be performed to indicate that the vapour column becomes unstable when $D_c k < 2$, with k being the wavenumber (Yao & Sun 1981). This instability condition represents the physical situation that the jet breaks into gas bubbles under the influence of surface tension when the wavelength exceeds the circumference of the jet, i.e. the Rayleigh instability. As the injection speed increases the jet becomes violent. This is known as the Helmholtz instability which causes flooding. In a semi-theoretical study on the hydrodynamic flooding criterion Yao & Sun (1982) select the Laplace length as the characteristic length, and point out that the two types of instability interact in such a way that the jet breaks at a distance from the orifice and bubbling occurs away from the gas inlet. The stable height of the gas column is determined by the cutoff wavelength in the vertical direction which, according to the same authors, coincides with the Taylor critical wavelength.

In order to quantify these ideas for the case of channels in a fluid-like behaving particulate, an effective density as well as an effective interfacial tension have to be defined. The first property is straightforward:

$$\rho_e = \rho_s(1 - \epsilon) + \rho_L \epsilon. \qquad [18]$$

For the second, one must consider that the pressure difference between the vapour and liquid phases is presently determined by the curvature of the menisci at the porous walls and not by the diameter of the jet, as in the previously mentioned analysis of Yao & Sun (1982). An effective interfacial tension that accounts for the increased capillary pressure can then be defined referring to [1], as follows:

$$\frac{2\sigma_e}{D_c} = \sigma \cos \theta \sqrt{\frac{\epsilon}{\kappa}} J_{br}. \qquad [19]$$

The resulting modified critical Taylor wavelength corresponding to the maximum stable L_c takes the form:

$$L_{c,m} = 2\pi \left[\frac{\sigma_e}{(\rho_e - \rho_G)g} \right]^{0.5}. \qquad [20]$$

This imposes a restriction for the L_c values given by [2] or [3], i.e. L_c values found using these relations are valid as long as they do not exceed the upper limit [20]. In a further step, one might also argue that the critical velocity at which the vapour jet becomes Helmholtz unstable (Chandrasekhar 1961),

$$V_{c,m} = \left(\frac{2\pi\sigma_e}{\rho_G L_{c,m}} \right)^{0.5}, \qquad [21]$$

gives, in combination with the number of channels per unit bed cross-sectional area, the dryout heat flux as the flooding limit is reached and no more downward liquid penetration and replenishment of the porous matrix is possible. The idea is investigated further in the section dealing with dryout in channelled beds.

The 10 cm high bed of ferrite particles (effective $d_p = 320 \, \mu$m) submerged in water and extensively tested in the Opera facility can be used as example. At dryout, the top 5 cm of the bed are traversed by 14–16 channels with an average D_c of 2.5 mm and these conditions appear to be fairly reproducible. The calculated maximum allowable $L_{c,m}$ by [20] is 4.85 cm, while the upward dryout heat flux found using [21] and the observed number of channels is $214 \pm 7\%$ kW/m², in good agreement with the experimentally measured $201 \pm 5\%$ kW/m².

A number of other observations can be explained by the present model. Barleon *et al.* (1984) report channels 4–5 cm long and 1 mm in diameter in a bed of 60 μm bronze particles submerged in water with top subcooling. Relations [2] and [3] suggest an L_c of about 15 cm when the prediction of $L_{c,m}$ based on [20] is 5.3 cm. Relatively stable channels were observed by Eckert *et al.* (1985) in thin test sections containing 30 μm nickel particles and water. They extended 4–7 cm inside the bed, depending on the thickness of the vessel—a variation that is attributed by the authors to possible non-uniformities in the heat production in the beds. Using the data in Abe *et al.* (1982) for the same beds, $L_{c,m}$ is estimated as 6.6 ± 0.5 cm, while the otherwise expected L_c would be around 13 cm. The power to reach dryout in both cases is quite low and no fluidization occurs, despite the very small particle sizes involved. A bed consisting of 435 μm steel particles in water has been tested at VKI by injecting air through its bottom support. The purpose is to observe any possible transition from stable channelling to fluidization and related channel instabilities for a bed characterized by large ρ_s. Channel depths of 2.5–4.0 cm and diameters of 1–2.5 mm, respectively, are typical for the usual PAHR gas flow rates. The extended L_c for this case, given by [2], is 3.75 cm. A most favourable $L_{c,m}$ prediction of 2.45–3.9 cm for the observed range of D_c is obtained from the proposed model. For quite high air velocities (>0.2 m/s), the channels become wide and particles are entrained by the gas stream. Secondary disturbances are also induced in a manner similar to the one already described for light particles.

It is interesting to note that [20] has been tried for several cases of solid–liquid combinations used in different out-of-pile tests, covering a wide range of the main parameters:

$$28 < d_p < 1100 \, \mu\text{m}, \quad 4700 < \rho_s < 10{,}500 \, \text{kg/m}^3,$$

$$0.018 < \sigma < 0.06 \, \text{N/m}, \quad 0.34 < \epsilon < 0.65.$$

The resulting values of $L_{c,m}$ never exceed 7.5 cm, in accordance with the experimental observations mentioned earlier that led to the idea of an existing maximum stable channel length.

The main uncertainty in the above calculations of $L_{c,m}$ comes from the value of D_c used. It is observed to be roughly proportional to the spacing between channels by Jones *et al.* (1984). Apart from the values quoted herein little information exists in the literature. Stubos & Buchlin (1988) report an average $D_c = 2.5$ mm for different glass, steel and ferrite beds in water and freon-113, the actual channel diameters ranging from 2.0 to 2.8 mm. The same average is suggested by Reed (1982) and Gabor *et al.* (1974), while Naik & Dhir (1982) observe channels with D_c varying between 1.9–4.1 mm in steel beds. Gladnick (1985) tested uniform glass beads with sizes from 0.5 to 3.0 mm

Table 1. Channel diameter D_c predictions for different systems

System	d_p (μm)	D_c (mm) [22], $C_0 = 20$	D_c (mm) [22], $C_0 = 50$	Exp. values
SS–water	780	1.65	2.55	$\leqslant 2.5$
SS–water (v)	690	1.7	2.65	1.9–4.0
SS–water (s)	780	1.4	2.2	$\leqslant 1.1$
Lead–water	930	1.4	2.2	$\leqslant 1.8$
Lead–water	780	1.45	2.3	$\leqslant 1.8$
Lead–water	460	1.5	2.4	$\leqslant 1.8$
Lead–methanol	460	0.95	1.5	$\leqslant 1.0$
SS–methanol	780	1.1	1.75	$\leqslant 1.1$
SS–isopropanol	780	1.1	1.75	$\leqslant 1.4$
Copper–water	1100	1.5	2.4	$\leqslant 1.6$
Copper–water	460	1.65	2.6	$\leqslant 1.6$
UO_2–water	210	1.8	2.85	≈ 3.0
UO_2–sodium	210	3.15	4.95	—
Ferrite–water (v)	320	2.25	3.5	≈ 2.5
Glass–water	500	2.5	3.95	≈ 1.0
Glass–water	1100	2.3	3.6	≈ 2.0
Glass–water	2000	2.2	3.5	≈ 2.5
Glass–water	3000	2.0	3.2	≈ 3.0
Bronze–water (v)	60	2.2	3.5	≈ 1.0
Bronze–water (v)	260	1.8	2.85	≈ 1.0

(v) = Volumetric heating; (s) = surfactant added.

Table 2. Channel length L_c predictions for the different in-pile tests

Experiment (date)	H (m)	d_p (μm)	Packed q (W/g)	Channelled q (W/g)	L_c, Lipinski (1982) (m)	L_c, present study (m)
D4 (1979)	0.0825	240	0.79	3.61	0.074	0.075
D10 (1984)	0.160	173	0.425	1.06	0.118	0.079
PIRAMID-1 (1986)	0.146	230	0.5	1.12	0.13	0.065

and measured D_c values of 1.0–3.75 mm, respectively. For shallow beds in water Dhir & Catton (1977) cite a value of 3.0 mm for D_c. In the case of a lack of relevant information, the aforementioned average of 2.5 mm can be used for the predictions along with a ±15% error band.

Employing a pipe flow analogy for the vapour flow through the channels and assuming that the vapour pressure drop corresponds to the available hydrostatic head, $\rho_e g L_c$, then

$$D_c = \frac{2f\rho_G V_c^2}{\rho_e g}$$ [22]

is obtained, with the friction factor f estimated for laminar vapour flow as

$$f = C_0 \frac{16}{Re};$$

Re being based on the D_c. As already discussed, a value between 10 and 50 seems appropriate for the coefficient C_0. Equation [22] allows for an estimation of D_c, with V_c found from [21]. It results in the correct order of magnitude, when compared with the available experimental data, as shown in table 1. Some of these data have been deduced from reported fractions of the bed cross-section occupied by the channels. Apart from offering a plausible justification of the observed magnitude of D_c in different systems, the table indicates that a value of 20 for C_0 gives a good estimation for most of the cases.

Another possible source of uncertainty in relation to the L_c estimation is the contact angle. Its effect is partially included in the Leverett function expression. The convention $\cos\theta = 1$ results in reasonable agreement between theory and experiments as far as the extended L_c is concerned and, therefore, it is adopted for general use in this study (Lipinski 1982).

It is of special interest to apply the present approach to the case of visually inaccessible in-pile tests, like D4 (Gronager et al. 1981), D10 (Mitchell et al. 1984) and PIRAMID-1 (Joly et al. 1988). Table 2 lists the main characteristics of the UO$_2$–sodium beds used at Sandia Laboratories and the nuclear center at Mol, Belgium. It also includes the predicted L_c by Lipinski as well as the present limiting channel length $L_{c,m}$. Early "natural" channelling is not observed and this has been accounted for by the already discussed sticking factor S_f concept. Superheat flashing of the liquid sodium (in D4) and sudden vapour production via steep power ramps (in D10 and PIRAMID-1) caused the penetration of vapour through the thick top-subcooled zone. The D4 bed, with an adiabatic bottom, is found to be almost entirely traversed by channels and, consequently, asks for an exceptionally high dryout power in comparison with the packed bed state. Similar observations should be made for the other two tests, according to Lipinski's predictions in table 2. However, the rather mild improvement in the bed coolability that resulted after the provoked channelling can be attributed to the significantly reduced $L_{c,m}$, which leaves a considerable part of the bed compact.

Before closing this section, it should be noted that when the effect of channels on the bed coolability is examined, attention has to be paid to the already mentioned presence of a cracked zone just below the channel base. This region, characterized by a thickness of 1–2 cm, is to be included to the disturbed part of the bed. Small cavities and nearly-horizontal cracks are observed there and their main function is to redistribute the vapour flow coming from the underlying packed zone and to feed the channels (Abe et al. 1982; Eckert et al. 1985; Buchlin et al. 1989).

DRYOUT IN CHANNELLED BEDS

The progress made regarding the modelling of channel behaviour allows for the investigation to proceed to the development of a complete model for the prediction of the dryout heat flux in channelled beds.

Dryout in Deep Channelled Beds

The most widely used model for the computation of the dryout heat flux in relatively deep channelled debris beds is the one first proposed by Lipinski (1982, 1984). With the requirement that the predicted L_c does not exceed half the bed height, so that the liquid and vapor flow resistances in the channelled zone can be assumed negligible compared to their packed region counterparts, the governing mass, momentum and energy balances are solved in the lower compact bed part to give the saturation profile along its axis. In this sense the incipient dryout heat flux can be found, provided that a value for the liquid fraction is available at the channel base. If the channelled zone can be considered subcooled because of the downcoming cool liquid, then a value of unity is the obvious choice. Otherwise, the continuity of the vapor pressure gradient at the packed/channelled zone interface may be employed as a boundary condition.

Within its application range the model performs satisfactorily, as long as the prevailing L_c is sufficiently well-estimated. The relations derived above offer a reliable value for L_c to be used for the dryout flux prediction. In summary, this approach links the packed and channelled parts of the bed and exemplifies the existing relation between channelled and packed dryouts. Indeed, the former can be considered as a subcase of the latter under the prescribed conditions of negligible flow resistances in the channelled zone. The modelling developed for the behaviour of the channels indicates the relative extent of the two zones and, therefore, can be used to decide if these conditions actually prevail in each individual case.

Although these considerations constitute an important step forward, they deal with only part of the entire problem. If the original hypothesis concerning the relative extent of the channelled zone in the bed is violated (e.g. the shallow channelled bed case), an apparent change in the mechanism causing dryout is reported (Dhir & Catton 1977; Jones et al. 1984). In the next section, devoted to dryout in shallow channelled beds, an attempt is made to devise a unified theory which takes into account experimental findings and the insight already gained.

Dryout in Shallow Channelled Beds

In the limit where the channels occupy the major part or even the whole packing, the packed region loses its dominant role and dryout in these shallow channelled beds is then governed by the channelled zone phenomenology. The understanding gained from the work described above on channel extent and stability is invoked for the development of proper physical modelling in this case too.

Shallow beds with channels extending to the bed bottom have received some attention, although most of the related studies involve bottom-heated cases (Gabor et al. 1974; Dhir & Catton 1977; Dhir & Barleon 1981; Jones et al. 1984). Using Taylor instability theory to predict the spacing between channels and Kelvin–Helmholtz instability theory to predict the maximum allowable vapour velocity through the channels, Jones et al. (1984) obtain the following modified form of Zuber's expression for the peak heat flux in pool boiling for use in predicting the dryout heat flux q_{bs} in bottom-heated shallow particulate beds:

$$\frac{q_{bs}}{h_{LG}\rho_G^{0.5}[\sigma g(\rho_e - \rho_G)]^{0.25}} = C_1,\qquad\qquad [23]$$

where the constant C_1 was determined by their experiments to be 0.035, and it is important to note the absence of any height dependence.

Dryout in shallow beds was also postulated by Dhir & Catton (1977) to occur when the vapour velocity in the channels exceeds the Kelvin–Helmholtz critical velocity. For the channel density, these workers applied a potential energy principle for the expanded channelled bed and presented an expression for the dryout heat flux as a function of bed height:

$$\frac{q_{bs}}{h_{LG}\rho_G^{0.5}[\sigma g(\rho_L - \rho_G)]^{0.25}} = C_2\left\{1 - C_3\frac{H(1-\epsilon)}{\left[\dfrac{\sigma}{g(\rho_L - \rho_G)}\right]^{0.5}}\right\};\qquad [24]$$

C_2 and C_3 being empirical constants.

The velocity at which the vapour jet in a channel becomes Helmholtz unstable is given by [21]. The dryout heat flux is expressed via the vapour flux and the latent heat:

$$q_{bs} = \frac{\pi D_c^2}{4} N_c h_{LG} \rho_G V_{c,m}.$$

[25]

After substituting [21] and [20], it becomes:

$$\frac{q_{bs}}{h_{LG} \rho_G^{0.5} [\sigma_e g (\rho_e - \rho_G)]^{0.25}} = \frac{\pi D_c^2}{4} N_c$$

[26]

The dryout heat flux in bottom-heated shallow beds can be calculated using [26], [22], [10] and [11]. In the case of volumetric heating, the channels are conical in shape and the maximum D_c is equal to $\sqrt{2}$ times the average one (Dhir & Catton 1977). If it is assumed that the friction factor and the effective surface tension are based on the mean D_c, the dryout heat flux for volumetrically heated beds is expected to be almost twice as large as that referring to the case of bottom heating (Dhir & Catton 1977). We say almost, because the existence of a top-subcooled zone in the bed may affect the conical shape of the channels.

Figure 12 compares the present model predictions to the bottom-heated test results from different authors. Fairly good agreement is noted for a wide range of the relevant parameters:

$$210 < d_p < 1100 \, \mu m, \qquad 7600 < \rho_s < 11400 \, kg/m^3,$$

$$0.018 < \sigma < 0.13 \, N/m, \qquad 0.4 < \epsilon < 0.5,$$

$$1.1 \, 10^6 < h_{LG} < 3.9 \, 10^6 \, J/kg, \qquad 740 < \rho_L < 1000 \, kg/m^3.$$

Limited data exist for volumetrically heated shallow beds. They are presented in figure 13 and lend further support to the present approach. The satisfactory prediction of the dryout heat flux for the D4 in-pile test verifies the postulation of channels extending to the bed bottom based on the improved modelling of L_c (cf. table 2).

Validation of the Complete Model

Figures 14–17 compare the complete model predictions with the data from several volumetrically heated systems, including the ferrite–water combination of the present study. Different liquids (water, freon-113) and solids (inductively heated bronze and steel, dielectrically heated ferrite) are
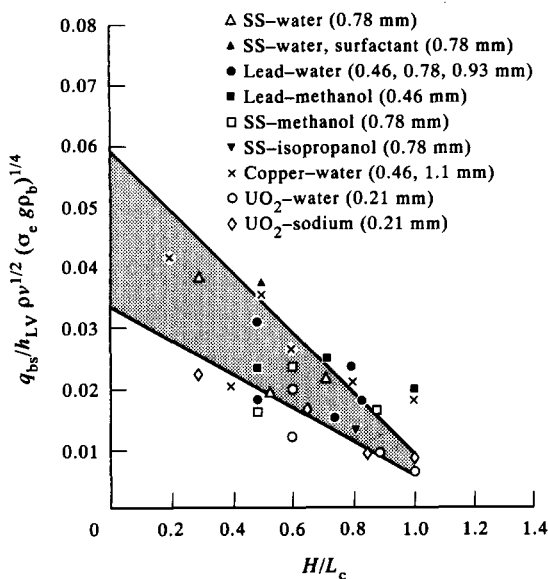
Figure 12. Dryout heat flux in shallow bottom-heated beds q_{bs}. The shaded area represents the model predictions for the different systems.
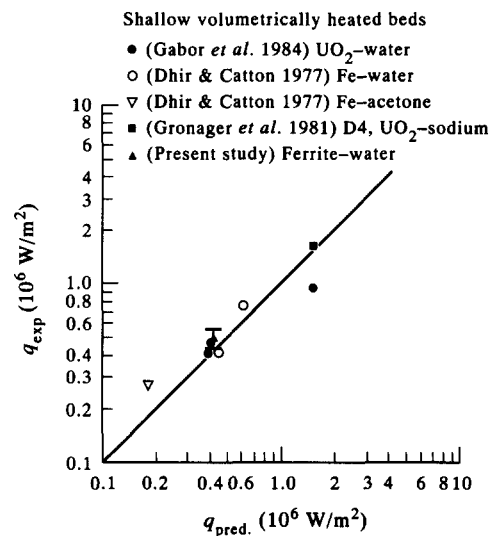
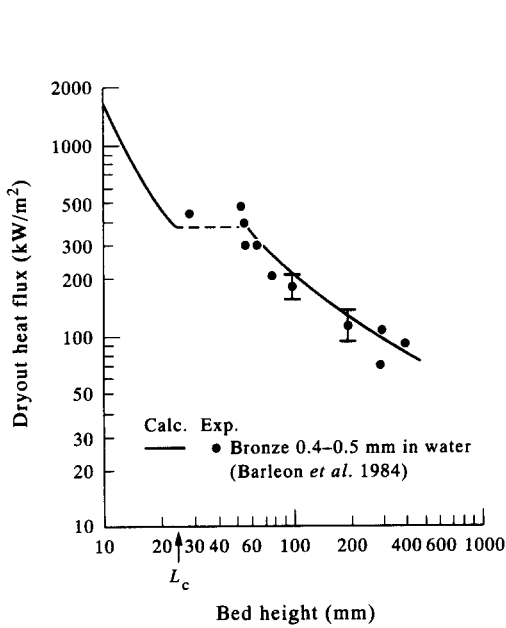Figure 13. Measured vs predicted dryout heat fluxes q in shallow volumetrically heated beds.

Figure 14. Dryout heat flux q vs bed height H: model predictions and experimental values for a bronze–water system.
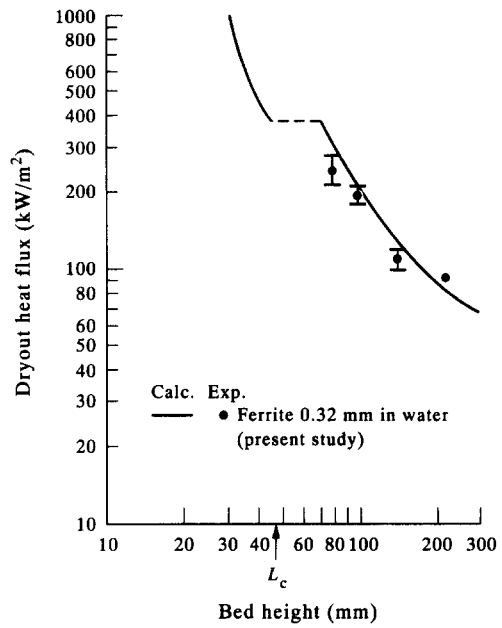
Figure 15. Dryout heat flux q vs bed height H: model predictions and experimental values from the present study.

involved, while the mean d_p ranges from 250 to 680 μm. The calculated L_c is shown in each individual figure.

In the case of H smaller than the predicted L_c, namely the shallow-bed limit, the respective part of the model takes over. The dryout heat flux computed at $H = L_c$ indicates the maximum power that can be removed by the fully, elongated channels. For smaller H, the number of channels N_c increases, [10], leading to higher dryout fluxes, [26].

When $H > L_c$, the deep channelled bed model dominated by the packed part is used. In all cases, as H decreases the dryout heat flux increases to the level represented by the dashed line. At this point the packed region has become small enough to be able to remove powers higher than the ones the overlying channels can possibly afford. In other words, the channelled zone starts playing
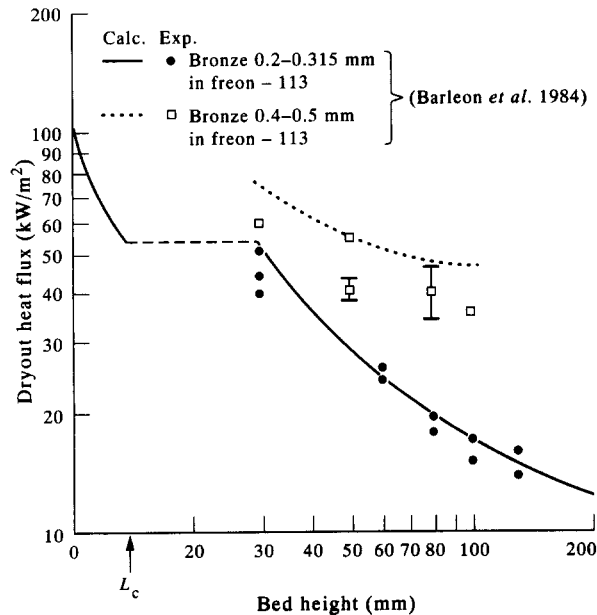

Figure 16. Dryout heat flux q vs bed height H: model predictions and experimental values for a bronze–freon-113 system.
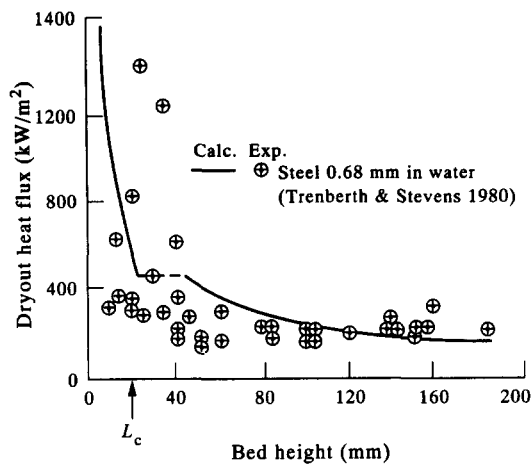
Figure 17. Dryout heat flux q vs bed height H: model predictions and experimental values for a steel–water system.

the main role if the bed depth is reduced further. It is important and encouraging to note that the extent of the dashed line is always of the order of the thickness of the cracked layer underlying the channelled region (≈ 2 cm). This observation represents the physical fact that dryout is imposed by the channelled zone for bed heights smaller than the thickness of the disturbed part of the packing (combined channelled ai.d cracked layers).

In view of the large scatter in the measurements, especially in the shallow-bed regime, and the complexity of the simulated disturbed zone phenomenology, it appears that the model performs satisfactorily in predicting dryout in out-of-pile channelled beds. The case of in-pile data should be examined also, as they form the ultimate validating element for the adopted modelling approach. Indeed, the results from the three tests in which bed disturbances occurred (D4) or were provoked (D10, PIRAMID-1) are shown in table 3, along the calculated L_c. The D4 bed can be considered shallow, while for the other two the deep-bed model is applicable (L_c of the order of half the bed height).

The successful predictions for the dryout power (table 3) indicate that the present model may explain the different relative enhancement of the bed coolability in seemingly similar systems.

CONCLUSIONS

The present investigation deals with the case of a particle bed, the upper part of which is characterized by the presence of low-resistance paths for the vapour escaping the packed boiling region. Their formation appears to be a necessary outcome of the porous flow equations, as long as it is accepted that the vapour phase may reach the bed top. Since they facilitate counter-current two-phase flow by allowing the passage of vapour through them and leaving the pore space for the downcoming liquid, these channels are expected to affect the coolability of the system.

The out-of-pile experimental study reveals for the first time the mechanisms of the different types of channel formation and suggests possible modelling approaches. The natural formation of channels in the bed can be modelled using the sticking factor S_f concept to account for the frictional forces that are important for incipient channelling. The provoked formation of channels is

Table 3. In-pile channelled dryout power predictions

Experiment (date)	H (m)	Packed q_{exp} (W/g)	Predicted L_c, present study (m)	Channelled q_{exp} (W/g)	Channelled q_{pred} (W/g)
D4 (1979)	0.0825	0.78	0.075	3.61	3.48
D10 (1984)	0.160	0.425	0.079	1.06	1.01
PIRAMID-1 (1986)	0.146	0.5	0.065	1.12 ± 0.05	1.18

attributed to Taylor instability, an important observation as far as the prediction of the number and pattern of channels is concerned.

After their formation (natural or provoked) the channels elongate to reach their extended length, which can be found from a balance between the vapour pressure and the overlying bed weight. Practically, the same result is obtained from the consideration of the statics of the channel wall in combination with the breakthrough value of the capillary pressure. This last approach is further explored in an effort to understand the behaviour of light particle beds. Fluidization becomes possible in this case and the similarities with other three-phase systems are noted. As channels are seen to become unstable under certain conditions, the problem of their stability is addressed in order to clarify discrepancies concerning heavy particle beds with large expected L_c. The maximum allowable stable channel length $L_{c,m}$ is determined in analogy with the stability of gas jets in a pool of liquid. The present approach, in comparison with the previous ones, predicts smaller stable L_c values when applied to the cases of in-pile tests, offering a plausible explanation for the observed mild enhancement of the bed coolability.

The improved modelling of channel behaviour helps in accomplishing the task initially set for the present study: the prediction of dryout in channelled beds. In fact, the most widely accepted idea for the estimation of the dryout heat flux refers to relatively deep channelled beds and simply assumes the dominant role of the packed region in imposing the dryout conditions. With the requirement that the predicted L_c does not exceed half the bed height, then one may simply resolve the packed part of the bed, the channelled zone offering only the top boundary condition. Within its application range this approach is found to perform fairly well as long as the prevailing is sufficiently well-estimated.

If the original hypothesis concerning the relative extent of the channelled zone in the bed is violated (e.g. a shallow channelled bed), an apparent change in the mechanism causing dryout is identified. On the basis of the limiting vapour velocity in the channels and the channel density correlation derived, a theoretical model for dryout in shallow channelled beds that requires no empirical coefficients is developed and successfully tested vs measured dryout fluxes.

Finally, the calculated dryout powers for different systems when plotted for a wide range of bed heights show good agreement with the experiments, validating the modelling approach for both the deep and shallow regimes. In addition, the results from the visually inaccessible in-pile tests are satisfactorily interpreted when the predicted L_c is used to categorize them in the respective bed regime.

REFERENCES

ABE, T., ECKERT, E. R. G. & GOLDSTEIN, R. J. 1982 A parametric study of boiling in a porous bed. *Warme- u. Stoffubert.* **16**, 119–126.

BARLEON, L., THOMAUSKE, K. & WERLE, H. 1984 Cooling of debris beds. *Nucl. Technol.* **65**, 67–86.

BARLEON, L., THOMAUSKE, K. & WERLE, H. 1985 Investigation on channel penetration at KfK. Paper presented at a *Mtg on Debris Bed Modelling*, Ispra, Italy.

BENOCCI, C., BUCHLIN, J-M. & JOLY, C. 1982 Boiling and dryout predictions in post accident heat removal situations. *Nucl. Technol.* **59**, 234–237.

BUCHLIN, J-M. & STUBOS, A. K. 1987 Phase change phenomena in liquid saturated self heated particulate beds. In *von Karman Institute Lecture Series 1988-01: Modeling and Applications of Transport Phenomena in Porous Media.*

BUCHLIN, J-M. & VAN KONINCKXLOO, T. 1986 O.P.E.R.A. II—a test facility to study the thermohydraulics of liquid saturated self heated porous media. von Karman Institute Report TM 41.

BUCHLIN, J-M., BENOCCI, C., JOLY, C. & SIEBERTZ, A. 1983 A two dimensional finite difference modeling of the thermohydraulic behaviour of the PAHR debris bed up to extended dryout. In *Post-Accident Debris Cooling; Proc. 5th PAHR Information Exchange Mtg* (Edited by MÜLLER, U. & GÜNTHER, C.). Braun, Karlsruhe.

BUCHLIN, J-M., STUBOS, A. K., DI FRANCESCO, M. & JOLY, C. 1989 Experimental and physical modeling of two-phase heat transfer in fuel debris beds. *J. Heat Technol.* **7**, 1–20.

CAMPOS, J. M. 1983 Theoretical and experimental investigation of channeled boiling in bottom heated particulate beds. von Karman Institute Report PR 1983-05.

CHANDRASEKHAR, S. 1961 *Hydrodynamic and Hydromagnetic Stability*. OUP, Oxford.

CHUOKE, R. L., VAN MEURS, P. & VAN DER POEL, C. 1959 The instability of slow immiscible viscous liquid–liquid displacements in permeable media. *Trans. AIME* **216**, 188.

DHIR, V. K. & BARLEON, L. 1981 Dryout heat flux in a bottom heated porous layer. *Trans. Am. Nucl. Soc.* **38**, 385–386.

DHIR, V. K. & CATTON, I. 1977 Study of dryout heat fluxes in beds of inductively heated particles. UCLA Report NUREG-0262 NRC 7.

ECKERT, E. R. G., GOLDSTEIN, R. J., BEHBAHANI, A. I. & HAIN, R. 1985 Boiling in an unconstricted granular medium. *Int. J. Heat Mass Transfer* **28**, 1187–1196.

GABOR, J. D., HESSON, J. C., BAKER, L. & CASSULO, J. C. 1972 Simulation experiments on heat transfer from fast reactor fuel debris. *Trans. Am. Nucl. Soc.* **15**, 836.

GABOR, J. D., SOWA, E. S., BAKER, L. & CASSULO, J. C. 1974 Studies and experiments on heat removal from fuel debris in sodium. Paper presented at the *ANS Fast Reactor Safety Mtg*, Beverly Hills, CA.

GABOR, J. D., CASSULO, J. C., FOUNTAIN, D. & BINGLE, J. D. 1984 Gas fluidization of solids in a stationary liquid. *AIChE Symp. Ser.* **80**(241), 95.

GLADNICK, P. G. 1985 Experimental investigation of channeling during boiling in liquid saturated porous media. von Karman Institute Report SR 1985-24.

GRONAGER, J. A., SCHWARZ, M. & LIPINSKI, R. J. 1981 PAHR debris bed experiment D4. Report NUREG/CR 1809.

JOLY, C. & LE RIGOLEUR, C. 1979 General and particular aspects of the particulate bed behaviour in the PAHR situation for liquid metal fast breeder reactors. In *von Karman Institute Lecture Series 1979-04: Fluid Dynamics of Porous Media in Energy Applications*.

JOLY, C., VERWIMP, A., BUCHLIN, J-M. & STUBOS, A. K. 1988 A complete PAHR programme in BR2, Mol, Belgium. Paper presented at the *Eur. Wkg Group on Irradiation Technology 30th Plenary Meeting*, Mol, Belgium.

JONES, S. W., BAKER, L., BANKOFF, S. G., EPSTEIN, M. & PEDERSEN, D. R. 1982 A theory for prediction of channel depth in boiling particulate beds. *J. Heat Transfer* **104**, 806–807.

JONES, S. W., EPSTEIN, M., BANKOFF, S. G. & PEDERSEN, D. R. 1984 Dryout heat fluxes in particulate beds heated through the base. *J. Heat Transfer* **106**, 176–183.

LIPINSKI, R. J. 1982 A model for boiling and dryout in particle beds. Sandia Labs Report SAND82-0765 (NUREG/CR-2646).

LIPINSKI, R. J. 1984 A coolability model for post accident nuclear reactor debris. *Nucl. Technol.* **65**, 53–66.

MEHR, K. & WURTZ, J. 1985 A model for the channeling of particle beds based on a parallel capillary tube approach. Ispra Joint Research Center Technical Note No. I.06.C1.85.166.

MITCHELL, G. W., OTTINGER, C. A. & MEISTER, H. 1984 Coolability of UO_2 with downward heat removal—the D10 experiment. Paper presented at the *6th Information Exchange Mtg on Debris Coolability*, UCLA, Los Angeles, CA.

NAIK, A. S. & DHIR, V. K. 1982 Forced flow evaporative cooling of a volumetrically heated porous layer. *Int. J. Heat Mass Transfer* **25**, 541–552.

REED, A. W. 1982 The effect of channeling on the dryout of heated particulate beds immersed in a liquid pool. Ph.D. Thesis, MIT, Cambridge, MA.

REED, A. W. 1986 A mechanistic explanation of channels in debris beds. *J. Heat Transfer* **108**, 125–131.

SCHWALM, D. 1985 Some remarks on channeling in particle beds. Ispra Joint Research Center Report EUR 10.005 EN.

SCHWALM, D. & NIJSING, R. 1982 The influence of subcooling on dryout inception in sodium-saturated fuel particle beds with top cooling and adiabatic bottom. *Nucl. Engng Des.* **70**, 201–208.

STEVENS, G. F. & TRENBERTH, R. 1982 Experimental studies of boiling heat transfer and dryout in heat generating particulate beds in water at 1 bar. UKAEA Winfrith Report AEEW-R 1545.

STUBOS, A. K. 1990 Boiling and dryout in unconsolidated particle beds. Ph.D. Thesis, Univ. Libre de Bruxelles–von Karman Institute, Rhode-St-Genese, Belgium.

STUBOS, A. K. & BUCHLIN, J-M. 1988 Modeling of vapour channeling behaviour in liquid saturated debris beds. *J. Heat Transfer* **110,** 968–975.

STUBOS, A. K. & BUCHLIN, J-M. 1993 Analysis and numerical simulation of the thermohydraulic behaviour of a heat dissipating debris bed during power transients. *Int. J. Heat Mass Transfer* **36,** 1391–1401.

STUBOS, A. K., PEREZ CASEIRAS, C., BUCHLIN, J-M. & JOLY, C. 1989 Numerical simulation of the transient thermohydraulic behaviour of a heat dissipating debris bed. *AIChE Symp. Ser.* **85**(269), 129–135.

YAO, L. S. & SUN, K. H. 1981 On the prediction of the hydrodynamic flooding criterion. Paper presented at *the 20th Natn. Heat Transfer Conf.,* Milwaukee, WI.

YAO, L. S. & SUN, K. H. 1982 On the prediction of the hydrodynamic flooding criterion. *J. Heat Transfer* **104,** 803–805.